



Evaluation of different types of carbonate aggregate performance in asphalt mixtures

Erfan Sadeghi¹ · Mohammad Reza Nikudel¹ · Amir Kavussi² · Mashallah Khamehchiyan¹

Received: 19 December 2021 / Accepted: 6 July 2022 / Published online: 25 July 2022
© Springer-Verlag GmbH Germany, part of Springer Nature 2022

Abstract

A comprehensive lithological and petrographic analysis of the aggregates gives information about the relationships between the aggregate properties and pavement performance. Although few studies have clearly established these relationships with various types of aggregates, they have not provided the effects of different types of carbonate aggregates. The purpose of this paper is to look at some aspects of the effects of different types of carbonate rocks on the performance of hot mix asphalt (HMA). Six types of aggregates that were evaluated in this study were collected from Central Alborz Zone (CAZ), one of the most important zones in Iran, and all of these were classified based on the petrographic study as carbonate rocks. This article has a deeper analysis of the rock material properties through a behavior analysis of asphalt mixtures subjected to boiling water, tensile strength ratio (TSR), semi-circular bending (SCB), and Cantabro tests. The most practical method for this purpose is to use microscopic thin sections of asphalt for evaluation of material properties on a small scale. Through an extensive laboratory program, the effects of aggregate properties on key mixture performance-based parameters such as adhesion, moisture susceptibility, fatigue, and durability are systematically summarized. The finding results show a classification for six different carbonate rocks based on their geological parameters. Also, a table is provided to aid in rock classification, indicating the most likely trend of each performance-based test result for carbonate rocks. Based on the Dunham classification for carbonate rocks, mud-supported materials have higher performance than grain-supported materials.

Keywords Central Alborz Zone · Carbonate rocks · HMA · Moisture susceptibility · Fatigue · Durability

Introduction

The HMA is considered the most widely used construction material for pavements. The HMA is a heterogeneous mixture of materials consisting of aggregates, bitumen, mineral fillers, and air voids. The effects of aggregate properties on the mechanical properties of HMA are essential in designing a high-quality pavement, so requires aggregates of multi-functional characteristics to meet various demands. These characteristics include stability, adhesion to bitumen, moisture susceptibility, crack resistance, and durability.

The stability of asphalt mixtures is difficult to understand due to its complex nature under different loading conditions

and internal factors. The mechanical strength of the asphalt pavements is directly related to the chemical interaction of mineral aggregates and binders (Ribeiro et al. 2009). Some researchers highlighted the influence of the mineralogical characteristics and interaction between aggregate and bitumen towards the long life of asphalt (Ribeiro et al. 2009; Liu and Jia 2011). Considering aggregate type, stability of mixture is higher for carbonate rocks such as limestone than other aggregate-type materials (Abo-Qudais and Al-Shweily 2007; Afaf 2014; Kavussi et al. 2014; Georgiou and Loizos 2014; Behiry 2015). Al-Suhaibani (1995) stated that limestone aggregates with low quality acquired high maximum Marshall stability and this could be misleading in many instances. Various researches have been associated with the binding between aggregates and binder surfaces to the stability of asphalt mixtures and chiefly with the loss of adhesion or stripping.

Many studies indicated that moisture damage, in form of stripping, is affected by the mineralogy of aggregate, the surface texture of aggregate, and the interaction between aggregate and binder. Moisture damage or moisture susceptibility

✉ Mohammad Reza Nikudel
Nikudelm@modares.ac.ir

¹ Department of Engineering Geology, Tarbiat Modares University, Tehran, Iran

² Department of Road and Transportation, Tarbiat Modares University, Tehran, Iran

can weaken the binder-aggregate interface resulting in adhesive failure. In general, aggregates with high carbonate content (CaCO_3) such as limestone form better adhesion with binder than aggregates with high silica content (Abo-Qudais and Al-Shweily 2007; Caro et al. 2008; Maiah and Al-Khateeb 2012; Zaumanis et al. 2018). Limestone aggregate contains less SiO_2 , which means that the HMA prepared using this material has a higher resistance to stripping compared to other aggregates. Silica usually causes a reduction in the bond between aggregate and binder. Bagampadde et al. (2005, 2006) investigated the impact of aggregate chemical composition on moisture susceptibility. The results indicated that there were no indications of moisture sensitivity in aggregates with calcium, magnesium, and iron, but aggregates containing alkali metals such as sodium and potassium exhibit relatively high moisture sensitivity.

Aggregates are commonly classified as either acidic or hydrophobic (water-repellent) and basic or hydrophilic (water-attracting) (Kanitpong and Bahia 2003; Bhasin 2006). The level of acidic or basic condition of each type of aggregates may vary according to their chemical composition. For instance, granite is classified as hydrophilic aggregate, and limestone is considered hydrophobic. In the order of acidic to basic (and thus from least adhesive to the most), aggregates can be roughly classified as quartzite, granite, sandstone, dolomite, basalt, limestone, and marble (D'Angelo and Anderson 2003). A number of methods have been successfully used to assess the moisture susceptibility of asphalt mixtures either on loose mixture (boiling water test) or compacted (TSR test) mixture for HMA (Ling et al. 2016; Kamran et al. 2021). Moisture damage can further lead to various distresses of pavement, including cracking.

Cracking is a predominant distress that frequently drives the need to rehabilitate asphalt pavements because of irreversible deficiencies, higher maintenance cost, and shorter serving lifespan (Yan et al. 2020; Liu et al. 2021). Fatigue cracking is caused by loss of adhesion between aggregate particles and asphalt binders or loss of cohesion in asphalt mixture or a combination of both mechanisms (Tan and Guo 2013; Taherkhani 2016; Cong et al. 2017; Kavussi and Naderi 2020). Basic aggregate such as limestone shows the weakness of binder cohesion which may cause microcracking in the pavement course and acid aggregate shows in such case weakness of adhesion that causes washing-up binder from aggregate and grain raveling (Birgisson et al. 2003). Al-Qadi et al. (2014) stated that the physical and chemical properties of aggregates and asphalt binders play a great role in the bond strength of the mixture and surface free energy (SFE), and the balance of these energies at the interface of binder-aggregate affect the bond strength. The SCB has been the most widely adopted due to its simplicity of sample preparation and the repeatability of test results (Fan et al. 2018; Ferjani et al. 2019). Durability is the ability

to withstand for a longer period without deterioration tendencies. Durability-related distresses more challenging to characterize than other distresses (e.g., rutting) but generally comprise non-load-associated cracking and raveling or weathering (Cox et al. 2017). The Cantabro durability test is used as an indirect measure of the potential for raveling and durability problems in asphalt mixtures. The Cantabro test is often used in the design of open-graded friction course mixtures (Watson et al. 2003; Wang et al. 2021) and dense-graded mixtures (Cox et al. 2017; Doyle and Howard 2011) as a measurement of durability.

The purpose of the present study is to evaluate a wide range of carbonate aggregate sources that have been approved by geological and engineering geological studies for applications in the HMA. The petrographic properties of six different carbonate rock formations, chosen between twelve formations depending on physical, mechanical, and durability characteristics, were quantified through quantitative and qualitative parameters. The main aims of this study comprise two major parts: (i) apply the innovative thin-section images of asphalt mixtures to evaluate the interaction between aggregates and bitumen in small scales; and (ii) classify different carbonate rocks based on their lithological properties in asphalt mixture performances. In order to evaluate the performance properties, boiling water test, TSR test, SCB test, and Cantabro test as well as microscopic studies were conducted.

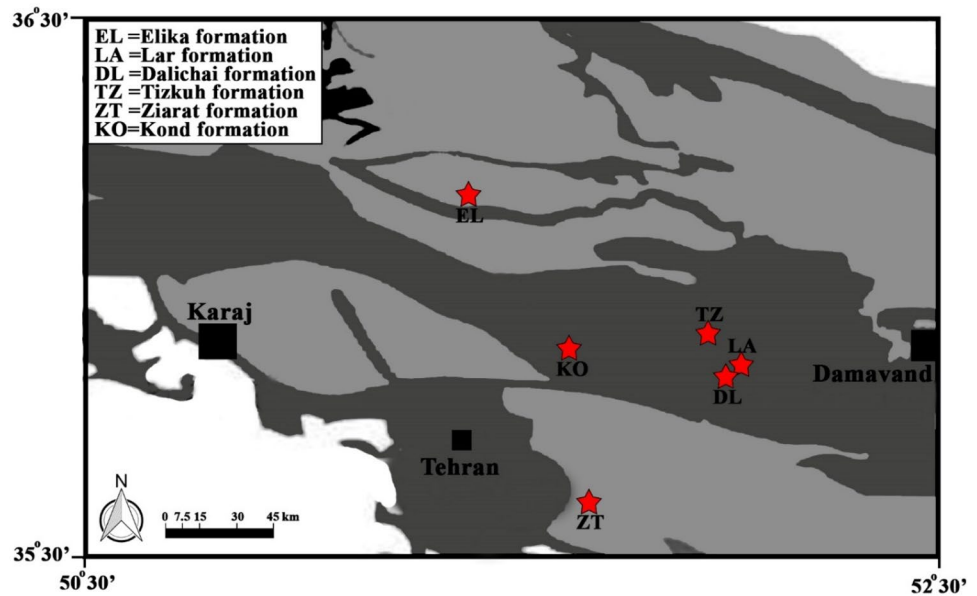
Study area

The CAZ is located at a latitude from $35^{\circ}30' \text{ N}$ to $36^{\circ}30' \text{ N}$ and a longitude from $50^{\circ}30' \text{ E}$ to $52^{\circ}30' \text{ E}$ and is a relatively vast area of about $20,000 \text{ km}^2$ (Fig. 1). There is a wide variety of rock formations and facies in the CAZ, characterized by the dominance of platform-type sediments, such as dolostone, limestone, and clastic rocks (Ghorbani 2013). This phenomenon highly affects the production of resources and rock materials. In the CAZ, there are six type sections of famous carbonate formations, used in different industries as material, including Elika, Dalichai, Lar, Tizkuh, Ziarat, and Kond (Table 1).

Geological setting

The tectonostratigraphic sequence of the CAZ comprises six carbonate formations in this study. The oldest one is the Elika Formation and includes brown thin-bedded, micritic, vermicular, alternating dolomites and limestones from lower and middle Triassic (Assereto 1996), which are overlain by middle to upper Jurassic sandy oolitic limestones, thinly bedded limestones, and ammonite bearing marls

Fig. 1 Geological and geographical locations of samples (six type sections of carbonate rocks of the CAZ)



interbedded with graywackes and shales of Dalichai Formation. The Lar Formation from the late Jurassic age includes thick-bedded, fossiliferous limestones (such as dismicrites and intrasparites). The Tizkuh Formation is characterized by the presence of the cliff-form of limey sandstone, polygenic conglomerate, and light orbitolina-bearing limestone of the Cretaceous succession of the CAZ. The Ziarat Formation includes thick-bedded reefal limestone and yellowish gypsiferous marl in the middle Eocene age, which are overlain by the youngest formation in this research, the Kond Formation, from the Late Eocene and includes alternation of gypsum, sandstone, conglomerate, marl, and limestone (Sadeghi et al. 2022a, b).

Methodology and materials

The research plan followed in this paper consists of extensive laboratory programs to determine the ability of different carbonate material performance in asphalt mixtures. This experimental study was carried out in three phases. The first phase of the study involved the aggregate selection based

on the geological and engineering geological test results. In the second phase, mix design was conducted based on the phase one results and Marshall tests, which were performed to evaluate the mixture stability, flow, and optimum binder content (OBC) for each type of aggregates. In the last phase of the study, in order to evaluate the performance properties, boiling water test for adhesion, TSR test for moisture susceptibility, and SCB test for fatigue as well as Cantabro tests for the durability of mixtures were conducted. Figure 2 shows the research outline flow chart defined for three phases in this research.

Aggregates

Six different carbonate aggregate types were obtained from the carbonate formations of the CAZ area (Fig. 1) and considered in this study: micrite (Elika), dolostone (Lar), bioclast packstone (Dalichai), bioclast packstone (Tizkuh), packstone-wackestone (Ziarat), and bioclastic grainstone (Kond). At the reconnaissance stage, thin sections of each rock type were examined and identified under the microscope. Also, in order to determine the type of rock, the

Table 1 Type section of carbonate rock formations of the CAZ

Formation name	Coordinate	Location	Total thickness (m)
Elika	N 36°09'13" E 51°24'26"	120 km north of Tehran in the south of Elika village	295
Lar	N 35°48'47" E 52°01'55"	80 km northeast to east of Tehran in the south of Damavand mountain	250–350
Dalichai	N 35°48'43" E 52°01'49"	80 km northeast to east of Tehran in the south of Damavand mountain	107
Tizkuh	N 35°52'21" E 52°00'39"	95 km northeast of Tehran in Tizkuh mountain	170
Ziarat	N 35°34'59" E 51°41'34"	50 km southeast of Tehran in Tochal village	450
Kond	N 35°52'47" E 51°39'04"	42 km northeast of Tehran in Kond-e-olya village	250

Fig. 2 Flow chart of the research outline

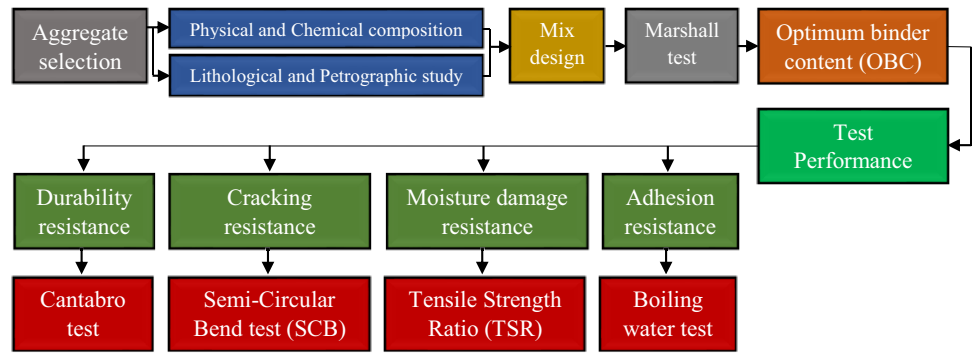


Table 2 Selected aggregate gradation

Sieve size (mm)	% passing	% retained	Coarse—fine	Size
19	100	0	54%	Coarse
12.5	90	10		
9	90	0		
4.75	46	44		
2.36	30	16	41%	Fine
1.18	30	0		
0.5	30	0		
0.3	8	22		
0.15	8	0		
0.075	5	3		
Filler (Pan)	0	5	5%	Filler

mineralogy was evaluated by the X-ray diffraction method. Aggregate gradation specifications were selected according to the Iranian Highway Asphalt Paving Code Number 234 (IHAP (Iran Highway Asphaltic Pavements) 2010). The selected aggregate gradation skeleton with the maximum nominal aggregate size (NMAS) of 19 mm consists of 54% coarse aggregates, 41% fine aggregates, and 5% filler (Table 2). The preliminary tests of the materials and the physical properties of the aggregates shown in Table 3 included an evaluation of the physico-mechanical

properties of the aggregates in terms of Los Angeles abrasion loss value (LAAV), stone density, unconfined compressive strength (UCS), specific gravity of aggregate, water absorption, elongation, and flakiness. The density of studied formations is classified based on the Anon (1979) classification as moderate density (2.45 g/cm³) and high density (2.61–2.72 g/cm³). According to ISRM (1981) and Deere and Miller (1966), intact rock classification for average values of UCS showed that all formations fall within the moderate class (20–60 MPa) to high class (60–200 MPa) and class D (28–56 MPa) to class C (56–112 MPa), respectively (Sadeghi et al. 2022a, b).

Asphalt binder

The asphalt binder PG 64–22 (60/70 penetration) was used as a virgin asphalt binder produced by Pasargad Oil Company to produce asphalt specimens. The properties of which are shown in Table 4.

Asphalt mixture design

The Marshall mix design was used in order to determine the stability, flow, and OBC of mixes based on the ASTM D1559. The specimens were compacted by 75 blows on each side with a Marshall hammer. A series of samples were

Table 3 Mechanical and physical properties of aggregates

Formation name	Stone density (g/cm ³)	UCS (MPa)	LAAV %	Specific gravity Coarse—fine	Water absorption Coarse—fine	Elongation %	Flakiness %
		ASTM D2938	ASTM C131	ASTM C127 ASTM C128	ASTM C127 ASTM C128		
Elika	2.69	55.52	22.38	2.67–2.69	0.32–0.28	9.72	20.08
Lar	2.72	58.37	22.04	2.63–2.64	1.28–1.27	16.93	12.16
Dalichai	2.64	82.32	16.00	2.64–2.65	0.46–0.44	7.38	25.99
Tizkuh	2.66	53.76	27.92	2.68–2.70	0.52–0.51	11.91	15.71
Ziarat	2.45	48.20	23.86	2.49–2.51	1.50–1.46	23.77	12.09
Kond	2.61	88.04	15.30	2.61–2.62	0.36–0.33	26.57	24.75

Table 4 Properties of the asphalt binder

Property (unit)	Standard	Analysis (value)	Specification	
			Min	Max
Density at 15 °C (kg/m ³)	ASTM D70	1.018	-	-
Penetration at 25 °C (100 g, 5 s) (dmm)	ASTM D5	60	60	70
Flash point (COC) (°C)	ASTM D92	250	232	-
Softening point (°C)	ASTM D36	52	49	56
Ductility at 25 °C (5 cm/min) (cm)	ASTM D113	100	100	-
Solubility in trichloroethylene (%)	ASTM D2042	99.6	99.5	-
Absolute viscosity at 60 °C (Pa·s)	ASTM D2171	336	-	-
RTFO mass loss (%)	ASTM D1754	-0.03	-	0.8

prepared and placed in a water bath at 60 °C for 30 min and then broken in a hydraulic compression test machine, which provide a loading rate of 50 mm/min. Marshall stability and flow values are determined from Marshall stability test results. According to the test results, the OBC was determined based on the average values of stability, flow, and air void content. The dosages of mixtures for carbonate rocks are shown in Table 5.

Test methods

The experimental program of the present research has been designed to properly show the effects of the aggregates in reaction with the bitumen and the applied loads. For these reasons, boiling water and TSR tests have been used to investigate the effect of the chemical composition of aggregates on their adhesion to bitumen and moisture susceptibility in the loose and compacted mixture for HMA. Also, in order to investigate the reaction of aggregates against the cracking and abrasion loss in asphalt mixtures, SCB and Cantabro resistance tests have been used, respectively.

Boiling water test

The boiling water test was specified in ASTM D3628 and employed to assess adhesion between aggregates and bitumen and water stability of asphalt mixtures. It is conducted

on loose mixtures to evaluate coating effectiveness by visually assessing the percentage of bitumen-coated area, which remained on aggregates after boiling. In this study, instead of using visual observation assessment, the digital imaging method for the evaluation of coating and potential moisture susceptibility was utilized. The original pictures were analyzed with ImageJ, an open-source image-processing program, by eliminating the background and calculating the area of coated and uncoated aggregates.

Tensile strength ratio test

Moisture susceptibility is the ability of mixtures to resist the stripping action, usually due to a reduction in cohesion strength within the asphalt binder and/or adhesion failure in the binder-aggregate system in the presence of water (Ziari et al. 2021). The indirect tensile strength (ITS) test was carried out according to the AASHTO T283 standard. This method consists of the change of diametral tensile resistance resulting from the effects of water saturation. According to the standard, three replicates were prepared for both the dry condition as unconditioned specimens and freeze–thaw cycle as conditioned specimens. The unconditioned specimens were transferred to a water bath for 2 h at 25 °C before the test. They were then put between the loading strips of a universal testing machine (UTM) and the ITS values of the samples were determined.

The conditioned specimens which contained 7 percent air voids were saturated using a vacuum pump with negative pressure to reach 55–80% saturation condition. These specimens were placed in a freezer at a temperature of -18 °C for 16 h. Then, the specimens were soaked in the water bath for 24 h at 60 °C, followed by soaking in water at 25 °C for 2 h. Finally, the conditioned specimens were put between the loading strips, and the ITS values of the samples were measured. The TSR was evaluated through the calculation of the ratio of the average ITS value for the conditioned specimens to the average ITS value for the unconditioned specimens as follows:

Table 5 The dosages of mixtures for carbonate rocks

Formation name	Unit proportion %			
	Bitumen	Coarse	Fine	Filler
Elika	5.82	50.86	38.61	4.71
Lar	5.82	50.86	38.61	4.71
Dalichai	5.86	50.84	38.60	4.71
Tizkuh	5.45	51.06	38.76	4.72
Ziarat	6.03	50.74	38.53	4.70
Kond	6.08	50.72	38.51	4.70

$$\text{TSR} = \frac{\text{ITS}_{\text{con.}}}{\text{ITS}_{\text{uncon.}}} \quad (1)$$

Semi-circular bending test

The SCB test is a laboratory mechanical test that uses semi-circular bending specimen geometry to evaluate the fracture resistance of asphalt mixtures at an intermediate temperature. The SCB test was carried out by following the procedure of [AASHTO TP124](#). The provisional standard test method calls for specimens with a diameter of 150 mm, a thickness of 50 mm, and a constant load-line displacement rate of 50 mm/min. The notch is 1.5 mm in width and 15 mm in length. SCB tests were conducted at 25 °C using a servo-hydraulic loading device, SANTAM UTM, which is equipped with a temperature-controlled chamber. The flexibility index (FI) was developed based on calculations of the measured fracture energy, which represented asphalt mixture capacity to resist cracking-related damage, and load-line displacement curve post-peak slope (m) values using Eq. (2):

$$\text{FI} = \frac{G_F}{\text{abs}(m)} \times A \quad (2)$$

where FI = flexibility index, G_F = fracture energy (J/m^2), m = absolute value of post-peak load slope m (kN/mm), and A = unit conversion and scaling coefficient taken as 0.01.

Cantabro test

The Cantabro loss test was used to evaluate the durability of asphalt mixtures. The Cantabro test was carried out referring to the [AASHTO TP108-14](#). A 150 mm diameter gyratory compacted specimen of nominal 115 mm height (controlled by the mass of mixture) was placed into a Los Angeles (LA) abrasion machine, following the general principles for use of a Los Angeles abrasion drum for 300 revolutions at 30–33 rpm without steel spheres at a temperature of 18 or 25 °C. Cantabro abrasion loss (CAL) was calculated by Eq. (3).

$$\text{CAL} = \frac{W1-W2}{W1} \times 100 \quad (3)$$

where $W1$ = initial mass of the specimen (g), and $W2$ = final mass of the specimen (g).

Results and discussion

The results of this study are presented and discussed in six separate sections, including petrographic study, asphalt thin section, Marshall test, moisture susceptibility, fatigue cracking resistance, and durability.

Petrographic study

The results of the petrographic analysis are summarized in Figs. 3 and 4, and Table 6. Based on the microscopic study, the Elika limestone matrix is composed of micrite (CaCO_3) and small amounts of fine-grain quartz that are scattered throughout the matrix (Fig. 4a). The rock's name is micrite (mudstone) and calcite, dolomite, and quartz are the main components (Table 6). The main components of the Lar Formation are dolomite minerals with a minor amount of calcite and quartz (Table 6). Dolomite minerals are in two forms including the zonation structure and the dusty core of minerals (most included). The Lar Formation is classified as dolomite/dolostone (Fig. 4b). The main components of the Dalichai Formation are skeletal fragments including pelagic bivalves and sponge needles. Some of these needles had been replaced by siliceous cement. According to X-ray results, the main components of Dalichai Formation rocks are calcite and quartz, which has the highest amount of quartz (29.02%) among the formations (Table 6). The Dalichai limestone is classified as Bioclast packstone (Fig. 4c).

The Tizkuh Formation is composed of skeletal fragments, crinoids, intraclasts, foraminifera, and *Orbitulina* fossils in a micrite cement. Some of the skeletal fragments are replaced by silica (Fig. 4d). The Tizkuh limestone is classified as bioclast packstone and the mineralogy of the rock is dominated by calcite in this formation (Table 6). The thin section of the Ziarat Formation shows skeletal fragments such as nummulite, algae fragments, and other foraminifera that spread in a micrite matrix (Fig. 4e). The Ziarat limestone is classified as packstone-wackestone and calcite, and quartz is the main component of rock types (Table 6). The main components of the Kond Formation are skeletal fragments including foraminifera, bivalvia, ostracod, and some plagioclase grains. The rock matrix is dolomitized and pyrite minerals have been replaced in the matrix and fossil structures (Fig. 4f). The Kond limestone is classified as bioclastic grainstone (Tuffaceous limestone), and based on the X-ray results, the main component of Kond Formation rocks are calcite and quartz (Table 6).

Asphalt thin section

Cubical HMA samples with a width of 25 mm, a height of 50 mm, and a thickness of 20 mm were used to prepare thin sections with a thickness of 30 μm for optical microscopy. These cubical HMA samples had to be impregnated with epoxy to protect their structure during sawing and polishing. The samples were placed under a vacuum pressure of 0.8 bars for impregnation of epoxy for a period of 1 h. Then, the samples were dried at room temperature for 24 h.

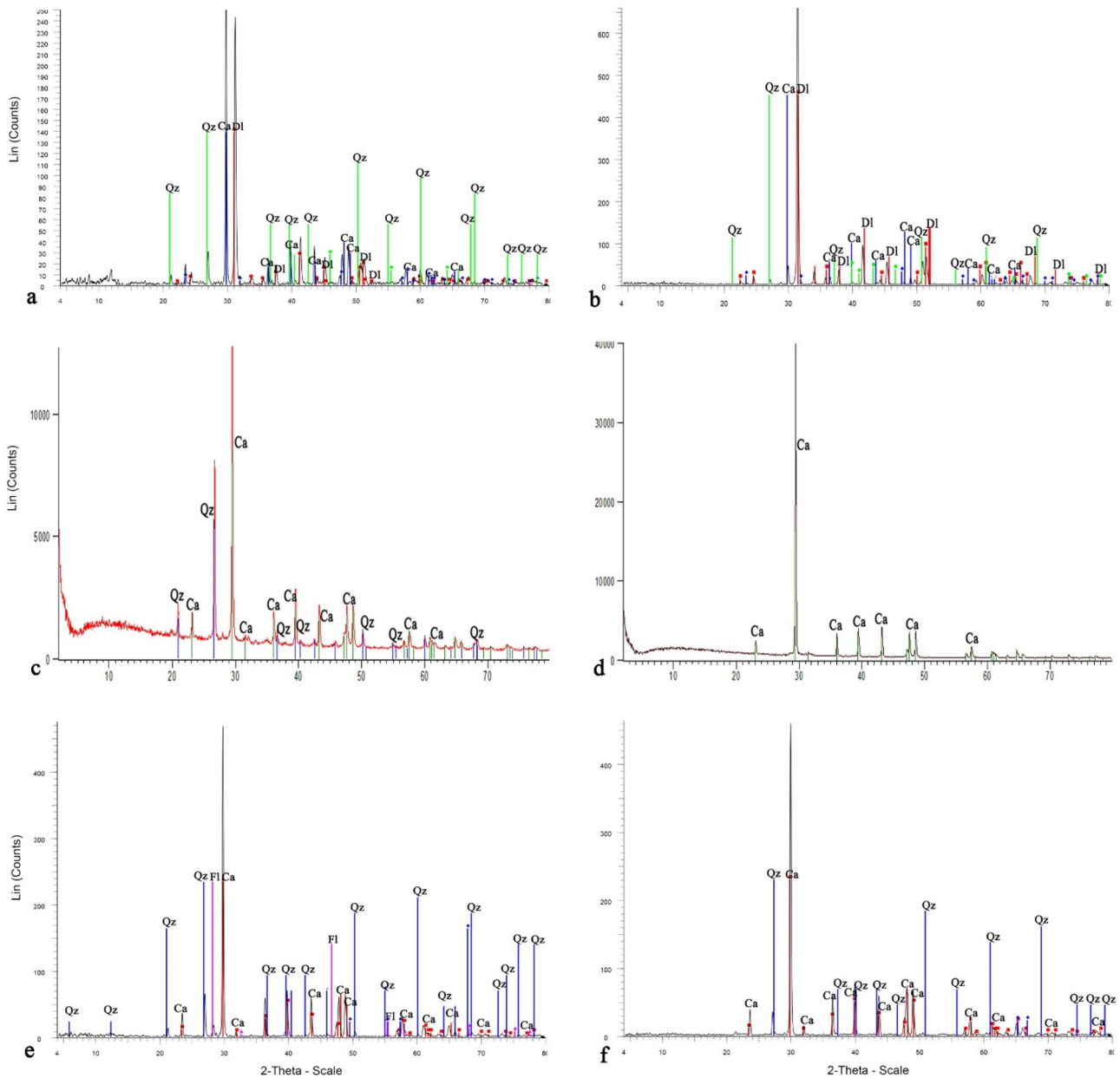


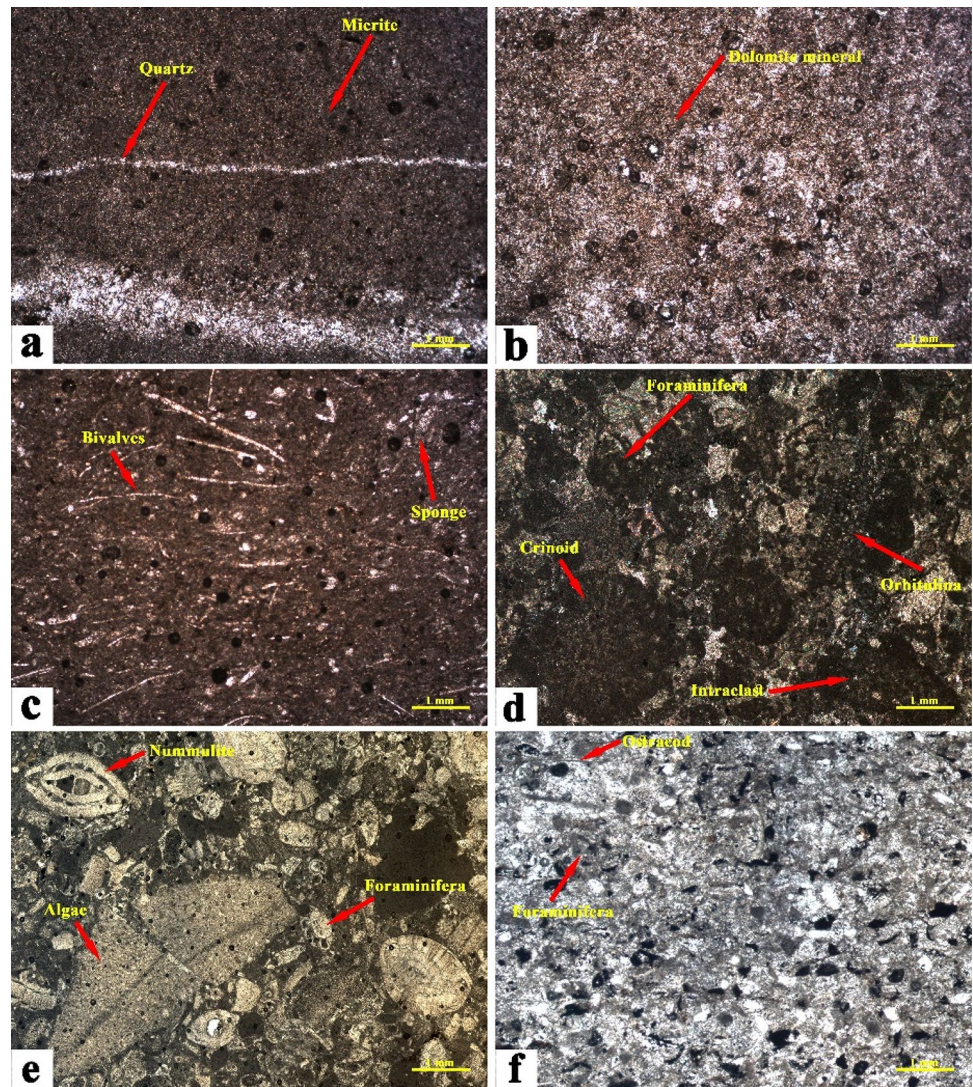
Fig. 3 XRD diffractograms of the CAZ, **a** Elika Formation, **b** Lar Formation, **c** Dalichai Formation, **d** Tizkuh Formation, **e** Ziarat Formation, **f** Kond Formation. Qz=quartz; DI=dolomite; Ca=calcite

To avoid crumbling, the samples were placed in a freezer at a temperature of -18 to -22 °C for 1 h, and during the sawing and polishing process, ice-cooled water was used. After polishing the first side of the samples, an object glass was glued to the polished surface and they were sawed very close to the glass. The final stage is polishing to a final thickness of 30 μ m by silicon carbide powders with grit sizes ranging from 100 to 1200 grit. The microscopic pictures of specimens are shown in Figs. 5, 6, 7, 8, 9, and 10.

Based on the microscopic study in the Elika limestone, angularity and surface roughness of the aggregates,

uniform distribution of different size aggregates, an adequate bond of bitumen around the aggregates, and low resistance of aggregates to grinding during the preparation stage are the most visible phenomena in the microscale (Fig. 5a). Also, the existence of fractures caused by testing (Fig. 5b) and the pre-existing microcracks filled by bitumen (Fig. 5c) are other apparent phenomena. The thin section of the Lar Formation shows angularity and surface roughness of the aggregates, lower flakiness and elongation, and uniform distribution of different size aggregates (Fig. 6a), Infiltration of bitumen into the aggregate

Fig. 4 Microscopic photographs of the CAZ, **a** Elika limestone (micrite), **b** Lar dolostone, **c** Dalichai limestone (bioclast packstone), **d** Tizkuh limestone (bioclast packstone), **e** Ziarat limestone (packstone-wackestone), **f** Kond limestone (bioclastic grainstone (tuffaceous limestone))



texture by selective absorption (Fig. 6b), and existence a large number of pre-existing microcracks in aggregates (Fig. 6c).

As can be seen from Fig. 7a, the Dalichai aggregates are flaky with lower surface roughness, angular aggregates, and uniform distribution of different size aggregates. Also, pre-existing microcracks filled by bitumen (Fig. 7b) and

the existence of many fractures caused by testing (Fig. 7c) are other apparent phenomena. In the Tizkuh Formation, angularity and surface roughness of the aggregates, uniform distribution of different size aggregates, an adequate bond of bitumen around the aggregates, and lower flakiness and elongation are the most visible phenomena in the microscale (Fig. 8a). Also, the existence of grain-boundary microcracks

Table 6 Semi-quantitative analysis by XRD and XRF of carbonate rocks. Qz, quartz; Dl, dolomite; Ca, calcite

Formation name	XRD	XRF								
		CaO	Co	MgO	SiO ₂	Al ₂ O ₃	Fe ₂ O ₃	K ₂ O	Na ₂ O	MnO
Elika	Ca, Dl, Qz	41.59	41.80	6.58	4.75	1.47	2.97	0.30	-	0.26
Lar	Dl, Ca, Qz	37.94	46.35	11.89	1.46	0.52	1.50	-	0.13	0.12
Dalichai	Ca, Qz	35.08	27.02	1.03	29.02	4.17	1.41	0.91	0.25	0.10
Tizkuh	Cal	55.52	43.14	0.31	0.47	0.22	0.10	-	-	0.08
Ziarat	Ca, Qz	53.35	41.30	0.35	4.08	0.26	0.18	0.05	0.10	0.18
Kond	Ca, Qz	48.81	36.16	0.52	10.26	1.87	1.26	0.08	0.46	0.22

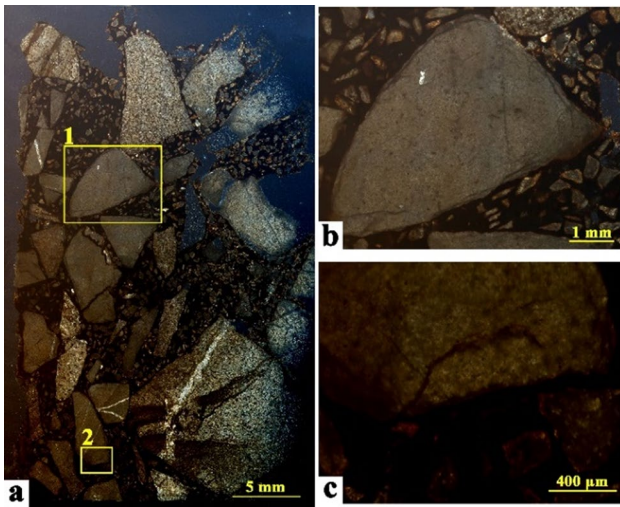


Fig. 5 Reference thin section of the Elika Fm., **a** microscopic images, **b** observation field 1, **c** observation field 2

between the large calcite minerals of the Tizkuh limestone (Fig. 8b) and the pre-existing microcracks (Fig. 8c) filled by bitumen are other apparent phenomena.

The thin section of the Ziarat Formation shows angularity and surface roughness of the aggregates, lower flakiness and elongation, an adequate bond of bitumen around the aggregates, and uniform distribution of different size aggregates (Fig. 9a), infiltration of bitumen into the fossil pores (Fig. 9b), and the existence of fractures caused by testing (Fig. 9c). The thin section of the Kond Formation illustrates surface roughness of the aggregates, higher flakiness and elongation, adequate bond of bitumen around the aggregates, uniform distribution of different size aggregates (Fig. 10a),

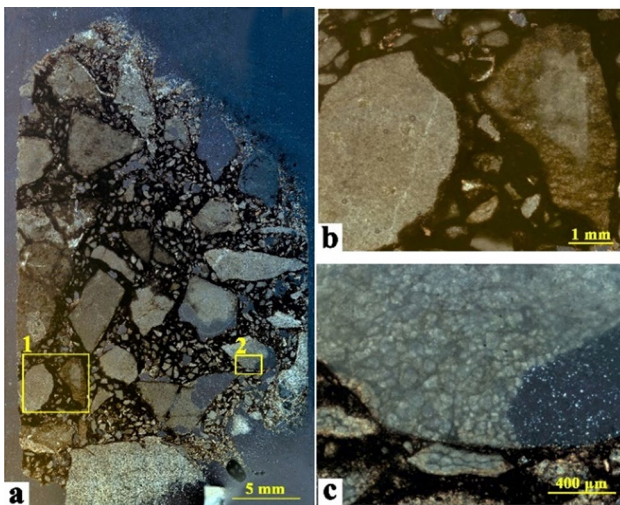


Fig. 6 Reference thin section of the Lar Fm., **a** microscopic images, **b** observation field 1, **c** observation field 2

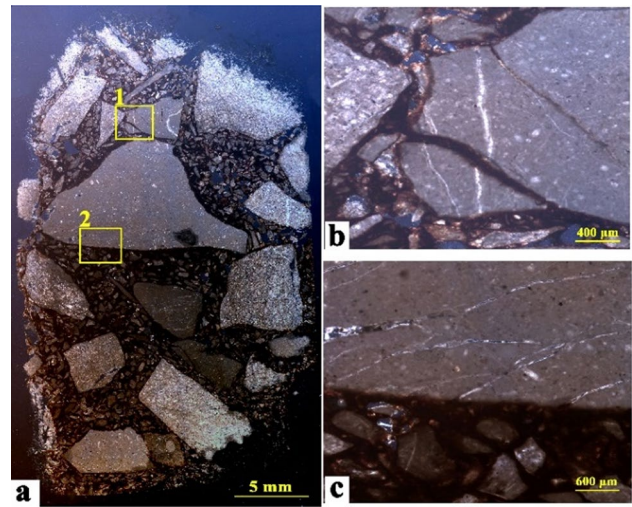


Fig. 7 Reference thin section of the Dalichai Fm., **a** microscopic images, **b** observation field 1, **c** observation field 2

the pre-existing microcracks filled by bitumen (Fig. 10b), and infiltration of bitumen into the aggregate texture by selective absorption (Fig. 10c).

Marshall test

The Marshall test was conducted to evaluate the stability and flow of mixtures and OBC of each aggregate type. As shown in Fig. 11, all asphalt mixtures met the requirements (Marshall stability > 7.8 kN) of Iranian standard IHAP Code 234 [40] for the Marshall test of mixes subjected to high traffic levels. The highest and lowest value of Marshall stability belongs to the Ziarat and Dalichai Formations, classified

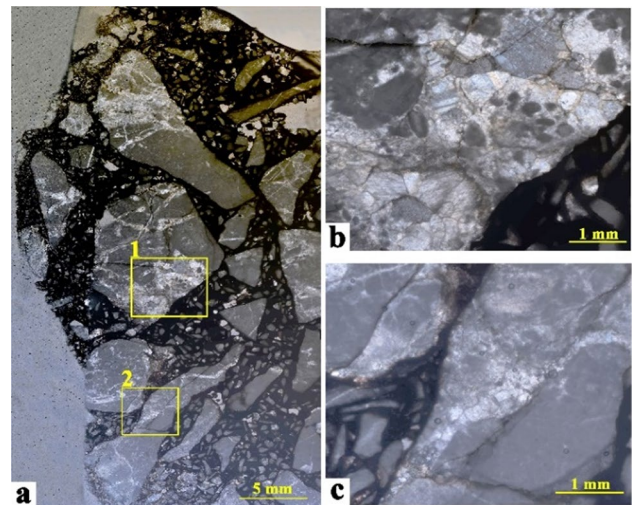


Fig. 8 Reference thin section of the Tizkuh Fm., **a** microscopic images, **b** observation field 1, **c** observation field 2

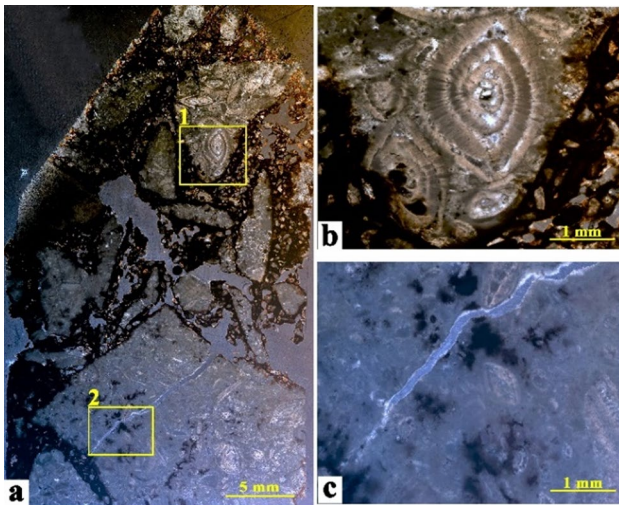


Fig. 9 Reference thin section of the Ziarat Fm., **a** microscopic images, **b** observation field 1, **c** observation field 2

as weak and strong rocks in mechanical tests such as UCS, respectively (Table 3). The Marshall stability was found to be highly correlated to a number of aggregate properties results such as the UCS test, LAAV test, and percentage of CaCO_3 and SiO_2 in the X-ray diffraction test (Fig. 12). As shown in Fig. 12, the stability increases with increasing LAAV and CaCO_3 values and decreasing the UCS and SiO_2 values. By comparing the Marshall stability with other test results, it can be seen that low-quality aggregates produced mixes with high Marshall stability, which could be misleading in many instances.

As shown in Fig. 11, the flow is obtained within the acceptable Iranian range (2–3.5 mm), except for the Elika

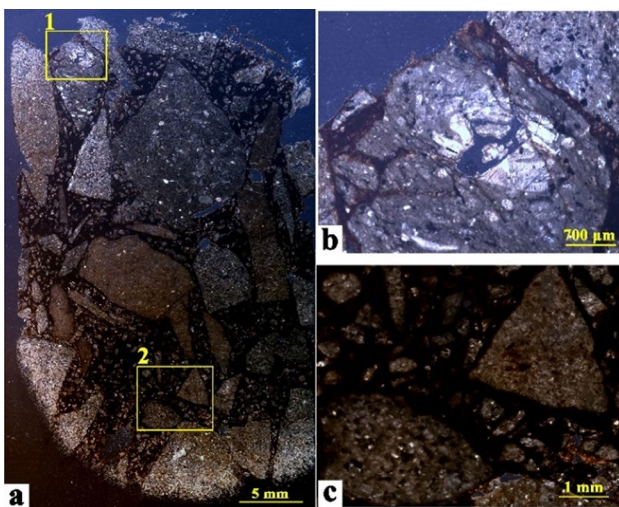


Fig. 10 Reference thin section of the Kond Fm., **a** microscopic images, **b** observation field 1, **c** observation field 2

Formation. The Elika and Lar Formations have the highest and the lowest values of Marshall flow, respectively. As can be seen from Table 3, Figs. 4a and 5, the Elika Formation has the lowest value of water absorption and its integrated structure (micrite) with few microcracks, which decrease the binder absorption ability of samples and aggregates could relocate easily. Furthermore, Table 3, Figs. 4b and 6 show the Lar Formation has a high value of water absorption, which causes infiltration of bitumen into the aggregate texture by selective absorption and a large number of grain-boundary microcracks due to the trigonal crystal system (Rhombohedral class) of dolomite minerals that causes a higher amount of spaces.

The OBC is selected as the average binder content for maximum stability, maximum density, and specified percent air voids in the total mix and plotted in Fig. 11. The OBC value for carbonate rocks ranges from 5.45 to 6.08%, and the difference in OBC value achieved by Tizkuh Formation could be related to the higher value of CaCO_3 (98.66%).

Moisture susceptibility

For determining moisture sensitivity of bitumen-aggregate mixtures, two tests were performed on loose mixtures (Boiling water test) and on compacted specimens (TSR test). In boiling water test, for the determination of the degree of the exposed area of aggregates, the original picture (Fig. 13a) was imported into ImageJ software. The first step is to eliminate the background by setting a specific value of the H, S, and B components. In this step, the pixels were classified based on their HSB value, in which the H and S components determine the chromaticity of color, and the B component refers to the luminance of the color. By eliminating the background, a non-classified image that represents the binder and aggregates is saved (Fig. 13b). The second step was to extract a classified image by eliminating the color component which represented the binder. Similarly to the first step, a specific combination of H, S, and B components is set so that the binder pixels are eliminated and only the aggregates remain (Fig. 13c). Then, the pixel area of exposed aggregates is calculated and the bitumen coverage values were determined (Fig. 14).

The ITS test, the other test for determining moisture susceptibility, was performed on all unconditioned (dry) and conditioned (wet) carbonate samples. The ITS test results are illustrated in Fig. 15. The Ziarat Formation has the highest value of unconditioned ITS test results and the lowest value in the conditioned ITS test results, which shows the biggest difference among formations. Similarly, the Lar Formation represents the same condition with a lower level of moisture susceptibility. On the contrary, the Tizkuh Formation has the best performance against moisture susceptibility. By correlating the boiling water test and TSR test results as shown in

Fig. 11 Marshall stability, flow, and OBC values of different carbonate formations

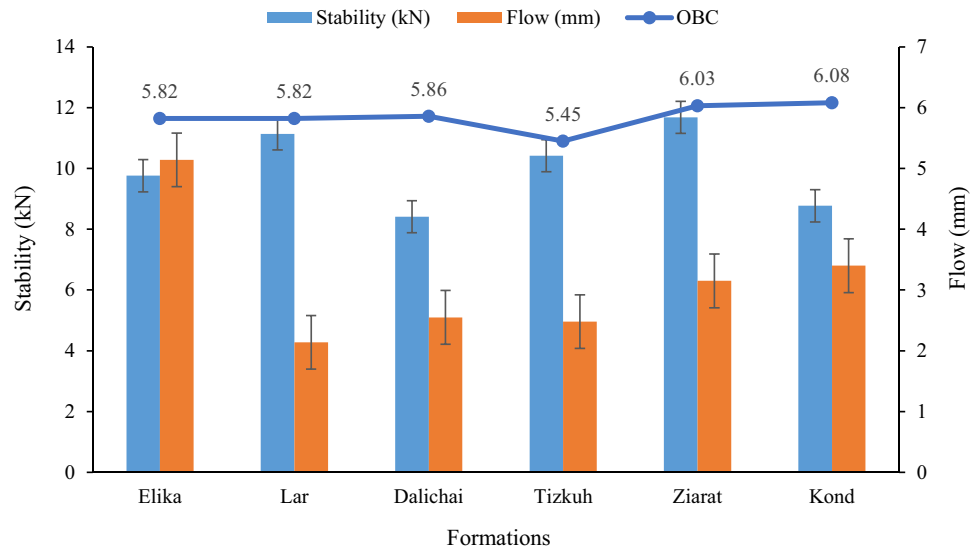


Fig. 16, it is seen that a very good correlation exists between quantitative boiling water test results and TSR, indicating the effectiveness of both methods in evaluating the moisture susceptibility values of loose and compacted asphalt mixtures.

As shown in Figs. 14 and 15, the Tizkuh Formation has shown higher values in TSR and boiling water test and best performance against moisture susceptibility, which is due to the highest percentage of CaCo₃ (approximately 98.7%) in its composition (Table 6). Also, the results show that despite the high percentage of SiO₂ in carbonate rocks of Dalichai and Kond Formations, these two formations have a relatively good performance against moisture sensitivity, which shows that quartz does not affect the test results. This result is in agreement with the study of Bagampadde et al. (2005), where it was concluded that moisture damage has no significant relationship with the contents of SiO₂. Although the Ziarat and Lar Formations have a good composition of CaCo₃ and MgO based on the X-ray diffraction tests, they obtain low values in TSR and boiling water test results. The low strength of these formations is one of the main reasons for lower resistance to moisture susceptibility because exposed uncoated surfaces of crushed aggregates can readily absorb water and initiate stripping. In this regard, Brown et al. (2009) stated that aggregates with low strength could

cause a moisture susceptibility problem if they are degraded during compaction or heavy traffic. Another reason is high water absorption in both formations, a high percentage of microcracks in the mineral structure of Lar Formation, and higher porosity in the Ziarat Formation fossils cause to absorb water into its structures and obtain higher moisture susceptibility.

Fatigue cracking resistance

The SCB test is a reliable method to evaluate the fatigue cracking resistance of HMA and also it benefits from easily prepared samples, simple setup and analysis, repeatability, and inexpensive test. The semi-circular specimens were prepared and tested under an SCB setup at intermediate temperature. The SCB tests were performed on the six different types of carbonate rocks and the vertical load–displacement curves of these tests are shown in Fig. 17. The displacement at failure can be employed to demonstrate the asphalt mixture properties before failure. According to the curves demonstrated in Fig. 17, the Ziarat Formation shows the highest peak load and the lowest deformation which indicates brittle behavior. On the contrary, the Elika Formation has the highest deformation and more viscoelastic behavior.

Fig. 12 a Relationship between Marshall stability (S_t) with UCS and SiO₂, **b** relationship between Marshall stability (S_t) with LAAV and CaCo₃

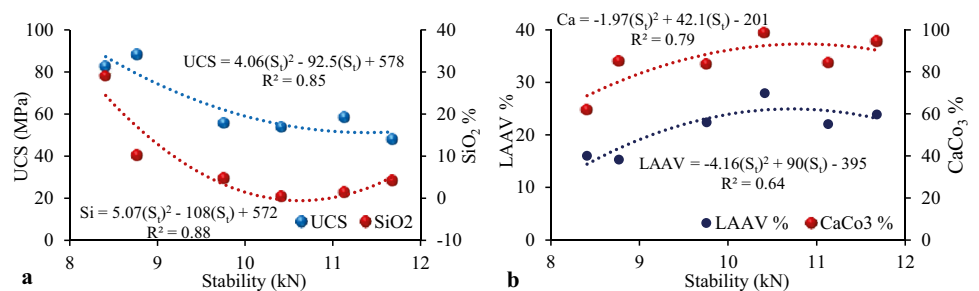


Fig. 13 **a** Original image of Ziarat Formation, **b** non-classified image, and **c** classified image

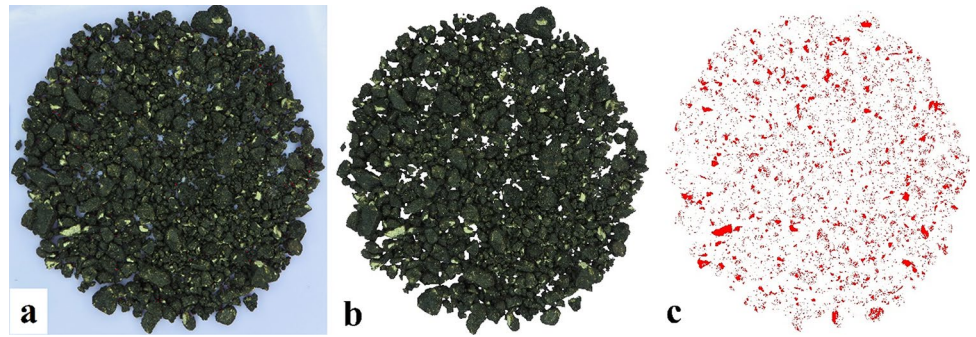


Fig. 14 Bitumen coverage values of different carbonate formations

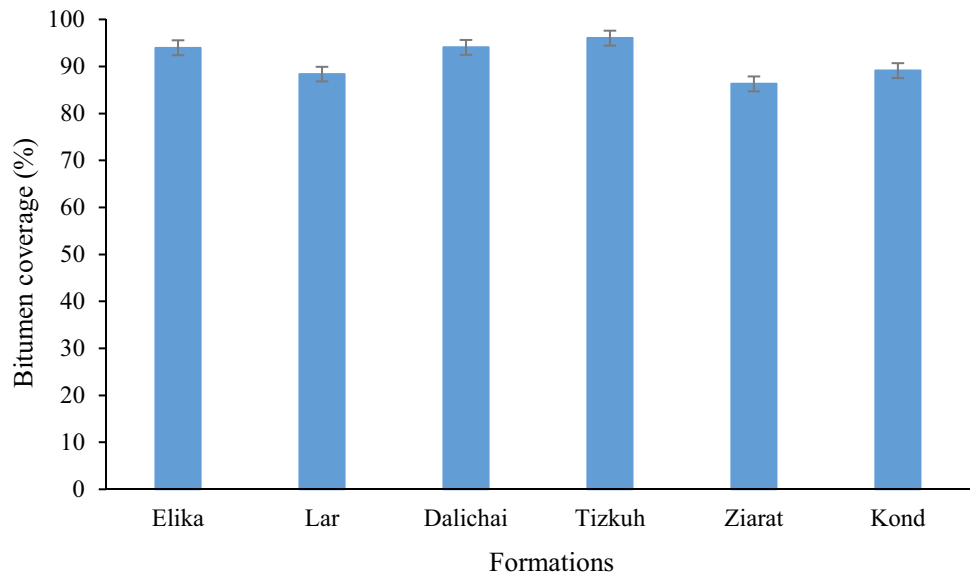


Fig. 15 Results of the indirect tensile strength of mixtures for different carbonate formations

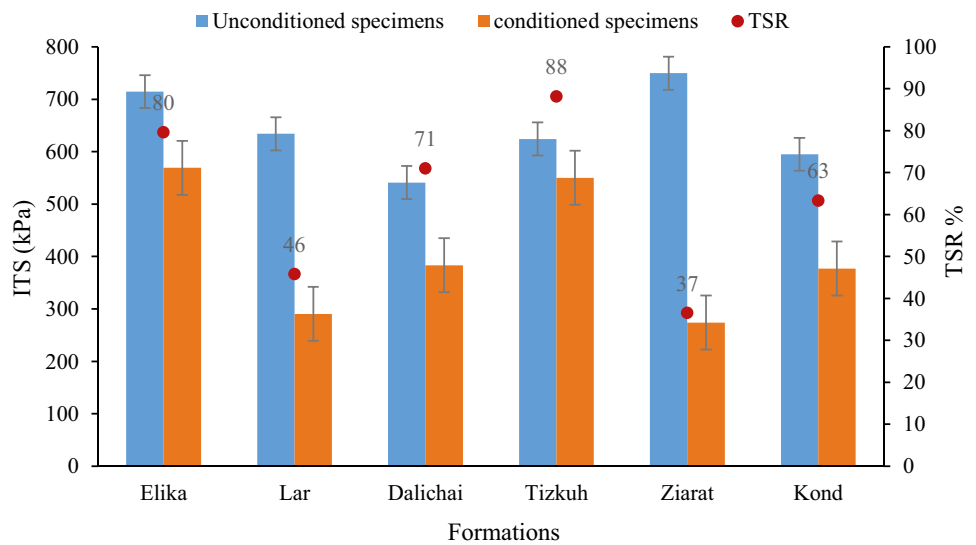
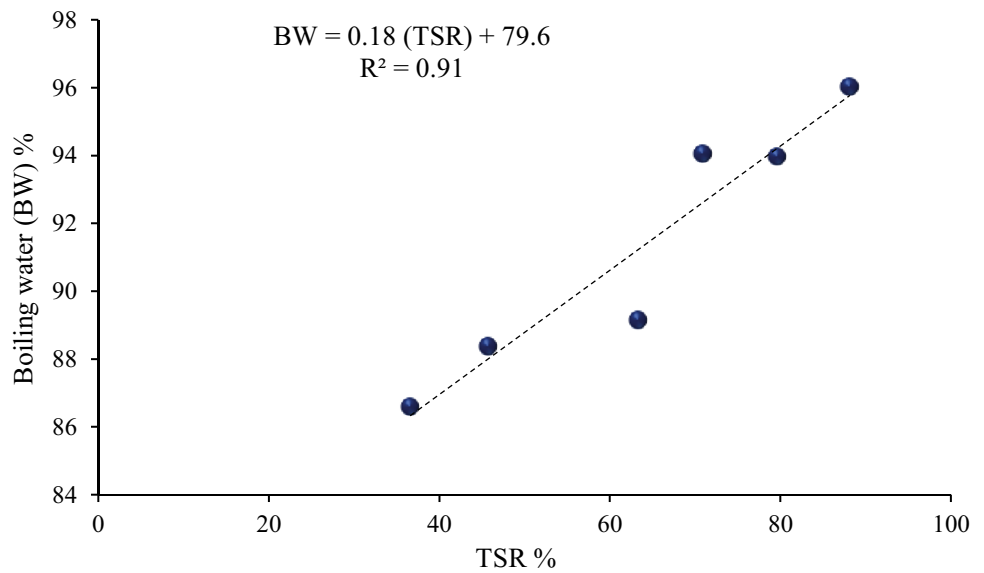


Fig. 16 Relation between the TSR and the boiling water test results



The load–displacement curves are used for calculating the fracture energy, post-peak slope, and flexibility index.

The fracture energy and flexibility index results of all carbonate formations are illustrated in Fig. 18. The Elika Formation shows higher fracture energy, which can be attributed to the strong bonding between limestone aggregates. Although the other formations have a different composition, they have relatively similar values of fracture energy. Also, the post-peak slope, which is known as a good parameter for correlating with crack propagation, is not fully in accordance with fracture energy to represent the classification of rock samples with respect to their potential cracking resistance. The flexibility index is more useful, due to the fact that the

mentioned parameters be combined to bring a reliable ranking.

According to the flexibility index, the best performing HMA mix is the Elika Formation with a flexibility value of 40.2 followed by Kond, Dalichai, Tizkuh, Ziarat, and Lar Formations from the highest to lowest values, respectively. The Elika Formation specimens have the lowest water absorption and porosity (Table 3 and Fig. 4) in their structure, so it is evident that has better viscoelastic behavior than other formations due to having enough binder film which may prevent cracking. The flexibility index of the Kond and Dalichai Formations is about half of the flexibility index of the Elika Formation, which higher water absorption and SiO₂

Fig. 17 Load–displacement curves of SCB tests

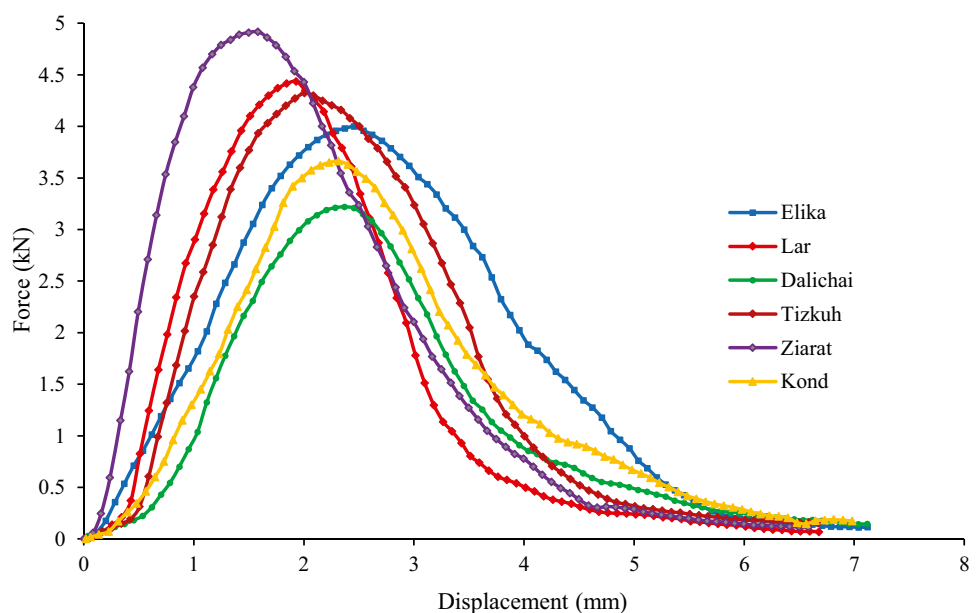


Fig. 18 Results of fracture energy and flexibility index of SCB tests

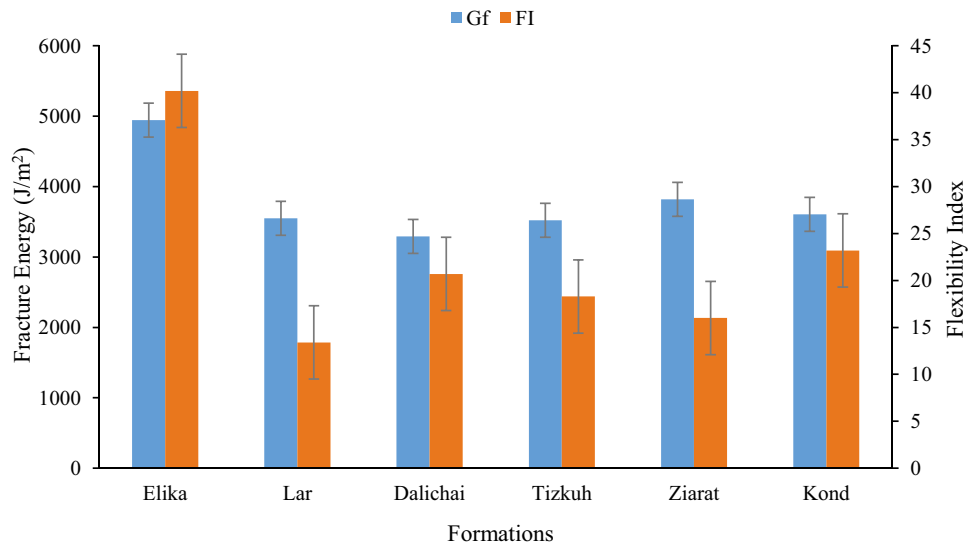


Fig. 19 Results of Cantabro loss test

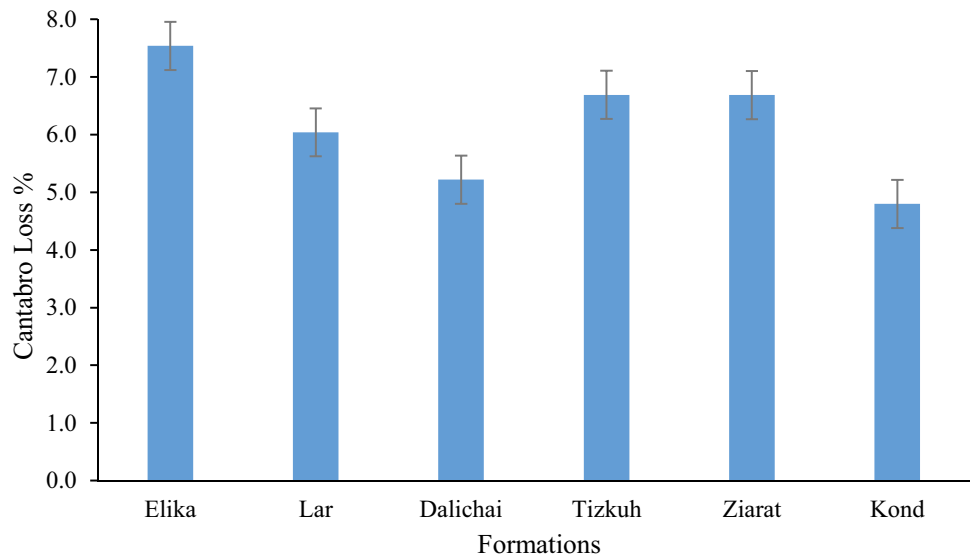
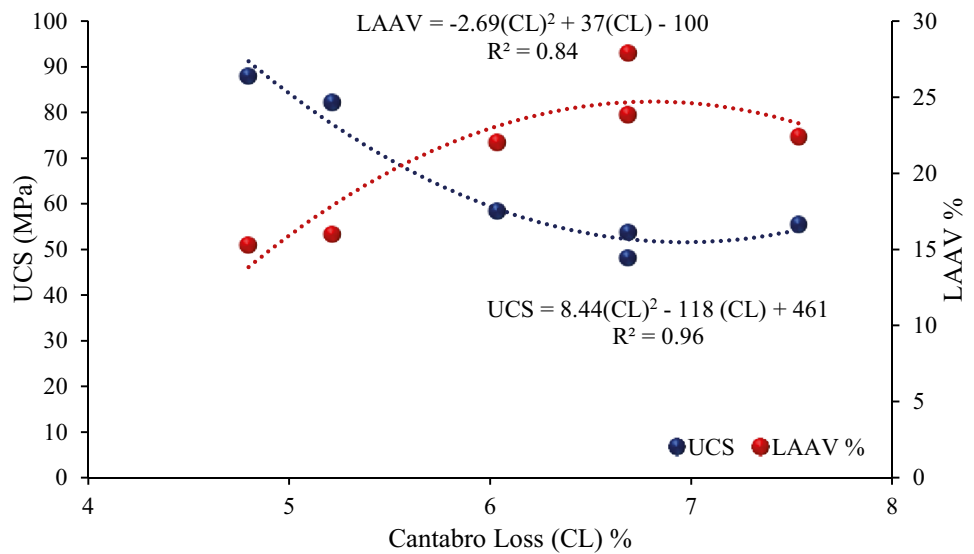


Fig. 20 Cantabro loss results versus UCS and LAAV



percentage could be the reasons for this difference (Tables 3 and 5). The higher percentage of SiO₂ leads to the higher strength of aggregates of these formations that causes it to behave elastically and exhibits negligible viscoelastic properties. The Tizkuh Formation absorbs bitumen into the mineral's grain-boundary microcracks, which reduces the thickness of bitumen film and viscoelastic behavior. As shown in Table 3, the Lar and Ziarat Formations show higher water absorption than other formations that cause the higher bitumen infiltration into aggregate pores by selective absorption (Figs. 6 and 9). With selective absorption, bitumen molecules are scattered inside the aggregate particles, which changes the material from a homogeneous to a heterogeneous material and turns the mechanical properties of limestone aggregates into viscoelastic materials from elastic materials (Lue

and Lytton 2013). However, it can be concluded that smaller molecular sizes of the solvent phase of binder, e.g., maltenes, are preferentially absorbed to aggregate pores by selective diffusion and left behind larger molecular species, e.g. asphaltenes (Lee et al. 1990; Curtis et al. 1993). The result of this postulated phenomenon with consequent changes in film properties is that asphalt becomes brittle and accelerates cracking, aging, and water damage.

Durability

Figure 19 shows the results of Cantabro durability testing of dense-graded asphalt mixtures. From Fig. 19, the Cantabro test could distinguish between different carbonate rocks of formations for hot mixed asphalt mixtures. Also, a strong

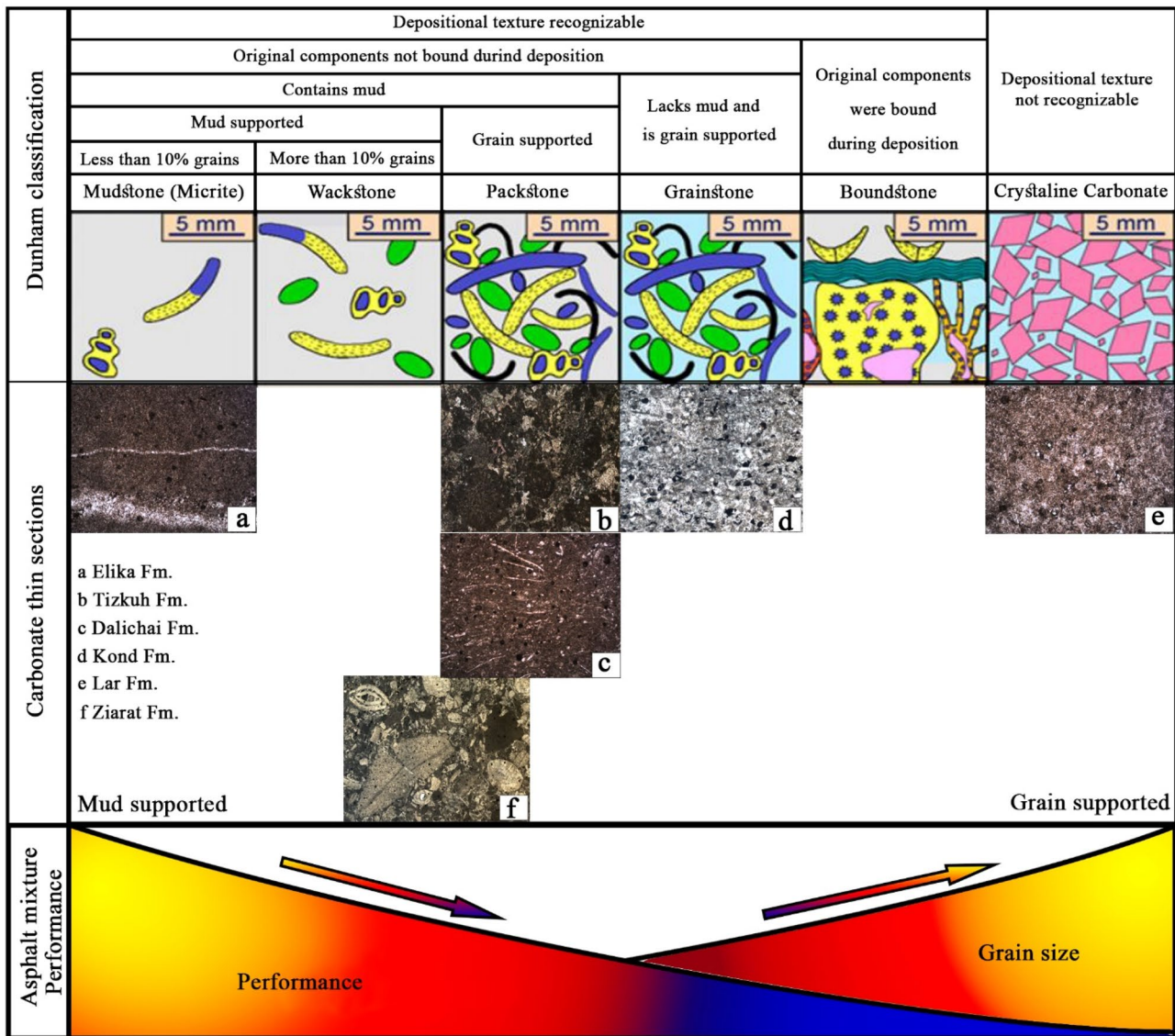





Fig. 21 Relationship between petrographic study and asphalt mixture performance

Table 7 Indication of change in performance-based test results for carbonate rocks

Formations	Stability (Marshal)	Moisture susceptibility (Boiling water)	Moisture susceptibility (TSR)	Cracking and Fatigue (SCB)	Durability (Cantabro)	Rank
Elika	→	↑	↑	↑	↓	1
Lar	↑	→	↓	↓	→	5
Dalichai	↓	↑	→	→	↑	3
Tizkuh	→	↑	↑	→	→	2
Ziarat	↑	↓	↓	↓	→	6
Kond	↓	→	→	↑	↑	4

 Good performance
 Medium performance
 Weak performance

relationship between the Cantabro test results with UCS and LAAV is observable (Fig. 20). As shown in Fig. 20, the Cantabro loss increases with increasing LAAV values and decreasing UCS values. The higher percentage of SiO₂ in the composition of the Dalichai and Kond Formations is the reason for lower values of Cantabro loss. The possible reason for the higher loss of the Elika Formation was that some of the aggregates fell apart rather than abrasion or breaking because of their integrated structure.

Summary

In this study, the effects of different types of carbonate rocks on the performance of asphalt mixtures were evaluated by conducting various tests. The overall trends from this study are summarized in Table 7. Based on the asphalt mixture performance, the most likely trend of each test result is captured, and the direction and color of arrows in the table are classified with regard to their performance (good, medium, weak). For each test, formations are divided into three groups with good, medium, and weak performance, which are indicated by green, yellow, and red arrows, respectively. The table can be used as a source of information for deciding which carbonate rock has higher performance in HMA. Carbonate rocks in this study are classified according to the type of lithology, which micrite (Elika), bioclast packstone (Tizkuh), bioclast packstone (Dalichai), bioclastic grainstone (Kond), dolostone (Lar), and packstone-wackestone (Ziarat) have the best to the weakest performance, respectively. The Dunham classification (Dunham 1962) scheme was used for the systematic description of carbonate rocks. Based on the Dunham classification for carbonate rocks, mud-supported materials have higher performance than grain-supported materials. This means that the asphalt mixture performance will decrease by increasing grain size and heterogeneity in rock texture (Fig. 21).

Conclusions

The purpose of this paper is to establish a relationship between the geological parameters of different types of carbonate rocks and hot mix asphalt (HMA) performance. In this investigation, the petrological properties of six types of aggregates were compared to the performance of their asphalt mixtures. The findings of this study can be summarized as follows:

1. Preparation of microscopic thin sections is a very useful resource for studying the small-scale features in the rock structure such as intragranular and grain-boundary microcracks, porosity, flakiness, elongation, surface roughness, and selective absorption.
2. The Marshall stability was found to be highly correlated to a number of aggregate properties such as the UCS test, LAAV test, CaCO₃, and SiO₂. Also, low-quality aggregates produced mixes with high Marshall stability, which could be misleading in many instances.
3. Low strength quality of aggregates, microcracks, and porosity has a higher effect on moisture susceptibility than the percentage of CaCO₃. In aggregates with a low amount of microcracks, the effect of CaCO₃ in preventing moisture susceptibility is higher. Moreover, moisture damage has no significant relationship with the contents of SiO₂.
4. Specimens with the lowest water absorption and porosity in their structure have better viscoelastic behavior. The higher percentage of SiO₂ leads to the higher strength of aggregates, elastic behavior, and negligible viscoelastic properties. The mineral's grain-boundary microcracks absorb bitumen which reduces the thickness of bitumen film and viscoelastic behavior. In aggregates with higher water absorption and selective absorption, materials change from homogeneous to heterogeneous and from elastic materials to viscoelastic materials. Aggre-

gate pores absorbed smaller molecular sizes by selective diffusion and left behind larger molecular species, so asphalt becomes brittle and accelerates cracking.

5. The Cantabro loss increases with increasing LAAV values and decreasing UCS values.
6. The six different carbonate rocks were classified based on their geological parameters. Carbonate rocks in this study are classified according to the type of lithology, which are micrite (Elika), bioclast packstone (Tizkuh), bioclast packstone (Dalichai), bioclastic grainstone (Kond), dolostone (Lar), and packstone-wackestone (Ziarat), and have the best to the weakest performance, respectively.

Acknowledgements The authors would like to thank Tarbiat Modares University for providing engineering geology laboratory and Roads and Transport laboratory facilities.

Declarations

Conflict of interest The authors declare no competing interests.

References

- AASHTO T 283–14 (2018) Standard method of test for resistance of compacted asphalt mixtures to moisture-induced damage. American Association of State and Highway Transportation Officials
- AASHTO TP 108–14 (2020) Describes the procedure for determining the percent abrasion loss of asphalt mixture specimens using the Los Angeles abrasion machine. American Association of State and Highway Transportation Officials
- AASHTO TP 124–20 (2020) Provisional standard method of test for determining the fracture potential of asphalt mixtures using Semi-circular Bend Geometry (SCB) at intermediate temperature. American Association of State and Highway Transportation Officials
- Abo-Qudais AS, Al-Shweily HA (2007) Effect of aggregate properties on asphalt mixtures stripping and creep behavior. *Constr Build Mater* 21(9):1886–1898
- Afaf AHM (2014) Effect of aggregate gradation and type on hot asphalt concrete mix properties. *J Eng Sci Assiut Univ Fac Eng* 42:567–574
- Al-Qadi IL, Abauwad IM, Dhasmana H, Coenen AR (2014) Effects of various asphalt binder additives/modifiers on moisture-susceptible asphaltic mixtures. Illinois Center for Transportation
- Al-Suhaibani AS (1995) Effect of aggregate properties on asphalt concrete mixes. *JKAU: Eng. Sci* 7:93–110
- Anon (1979) Classification of rocks and soils for engineering geology mapping, part 1: rock and soil material. *Bull Assoc Eng Geol* 19:355–371
- Assereto R (1966) Explanatory notes on the geological map of upper Djadgerud and Lar valleys (Central Alborz, Iran), Series G., publication no. 232. Institute of Geology of the University of Milan, Italy
- ASTM C127–15 (2015) Standard test method for relative density (specific gravity) and absorption of coarse aggregate. ASTM International, West Conshohocken, PA
- ASTM C128–15 (2015) Standard test method for relative density (specific gravity) and absorption of fine aggregate. ASTM International, West Conshohocken, PA
- ASTM C131–20 (2020) Standard test method for resistance to degradation of small-size coarse aggregate by abrasion and impact in the Los Angeles machine. ASTM International, West Conshohocken, PA
- ASTM D2938-95 (2002) Standard test method of unconfined compressive strength of intact rock core specimens. ASTM International
- ASTM D113–17 (2017) standard test method for ductility of asphalt materials. ASTM International, West Conshohocken, PA
- ASTM D1559–89 (1998) Test method for resistance of plastic flow of bituminous mixtures using marshall apparatus (Withdrawn 1998). ASTM International, PA
- ASTM D1754–20 (2020) Standard test method for effects of heat and air on asphaltic materials (thin-film oven test). ASTM International, West Conshohocken, PA
- ASTM D2042–15 (2015) Standard test method for solubility of asphalt materials in trichloroethylene. ASTM International, West Conshohocken, PA
- ASTM D2171–18 (2018) Standard test method for viscosity of asphalts by vacuum capillary viscometer. ASTM International, West Conshohocken, PA
- ASTM D36–14 (2020) Standard test method for softening point of bitumen (ring-and-ball apparatus). ASTM International, West Conshohocken, PA
- ASTM D3628–15 (2021) Standard practice for selection and use of emulsified asphalts. ASTM International, West Conshohocken, PA
- ASTM D5–20 (2020) Standard test method for penetration of bituminous materials. ASTM International, West Conshohocken, PA
- ASTM D70–21 (2021) Standard test method for specific gravity and density of semi-solid asphalt binder (pycnometer method). ASTM International, West Conshohocken, PA
- ASTM D92–18 (2018) standard test method for flash and fire points by Cleveland open cup tester. ASTM International, West Conshohocken, PA
- Bagampadde U, Isacson U, Kiggundu B (2005) Influence of aggregate chemical and mineralogical composition on stripping in bituminous mixtures. *Int J Pavement Eng* 6:229–239
- Bagampadde U, Isacson U, Kiggundu B (2006) Impact of bitumen and aggregate composition on stripping in bituminous mixtures. *Mater Struct* 39:303–315
- Behiry EM (2015) Optimisation of hot mix asphalt performance based on aggregate selection. *Int J Pavement Eng* 17(10):924–940. <https://doi.org/10.1080/10298436.2015.1043634>
- Bhasin A (2006) Development of methods to quantify bitumen-aggregate adhesion and loss of adhesion due to water. PhD thesis. Texas A&M University, College Station
- Birgisson B, Roque R, Page GC (2003) Evaluation of water damage using hot mix asphalt fracture mechanics. *J Assoc Asphalt Paving Technol* 72:424–462
- Brown R, Kandhal PS, Roberts FL, Kim RY, Lee DY, Kennedy TW (2009) Hot mix asphalt materials, mixture design, and construction, NAPA, Lanham, MD
- BS 812–105.1 (1989) Testing aggregates. Methods for determination of particle shape. Flakiness index, BSI
- BS 812–105.2 (1990) Testing aggregates. Methods for determination of particle shape. Elongation index of coarse aggregate, BSI
- Caro S, Masad E, Bhasin A, Little DN (2008) Moisture susceptibility of asphalt mixtures, part 1: mechanisms. *Int J Pavement Eng* 9(2):81–98
- Cong L, Peng J, Guo Z, Wang Q (2017) Evaluation of fatigue cracking in asphalt mixtures based on surface energy. *J Mater Civ Eng* 29(3):D4015003
- Cox BC, Smith BT, Howard IL, James RS (2017) State of knowledge for Cantabro testing of dense graded asphalt. *J Mater Civ Eng* 29(10):04017174
- Curtis CW, Ensley K, Epps J (1993) Fundamental properties of asphalt-aggregate interactions including adhesion and absorption.

- Strategic Highway Research Program (SHRP) Rep. No. SHRP-A-341, National Research Council, Washington, DC
- D'Angelo J, Anderson RM (2003) Material production, mix design, and pavement design effects on moisture damage. The National Academies Press, Moisture Sensitivity of Asphalt Pavements
- Deere DU, Miller R (1966) Engineering classification and index properties for intact rock: Technical Report on Air Force Weapons Lab. 65-116, New Mexico, No. AFWL-TR
- Doyle JD, Howard IL (2011) Evaluation of the Cantabro durability test for dense graded asphalt. Proc., Geo-Frontiers 2011 (GSP 211), ASCE, Dallas, 4563–4572
- Dunham RJ (1962) Classification of carbonate rocks according to depositional texture. *Am Assoc Pet Geol* 11:108–121
- Fan S, Wang H, Zhu H, Sun W (2018) Evaluation of self-healing performance of asphalt concrete for low-temperature fracture using semicircular bending test. *J Mater Civ Eng* 30(9)
- Ferjani A, Carter A, Vaillancourt M, Dardeau A, Gandi A (2019) Effect of cement content on cracking resistance of full-depth reclamation materials using the semicircular bending test. *Adv Civ Eng Mater* 8(1):411–422
- Georgiou P, Loizos A (2014) A laboratory compaction approach to characterize asphalt pavement surface friction performance. *Wear* 311(1–2):114–122. <https://doi.org/10.1016/j.wear.2013.12.028>
- Ghorbani M (2013) The economic geology of Iran, mineral deposits and natural resources. Springer, Netherlands
- IHAP (Iran Highway Asphaltic Pavements) (2010) Iran Management and Planning Organization, Code 234, Tehran, Iran, 2nd edition
- ISRM (1981) Rock characterization testing and monitoring, ISRM suggested methods. Commission on testing methods. International Society for Rock Mechanic
- Kamran F, Basavarajappa M, Bala N, Hashemian L (2021) Laboratory evaluation of stabilized base course using asphalt emulsion and asphaltenes derived from Alberta oil sands. *Constr Build Mater* 283:122735. <https://doi.org/10.1016/j.conbuildmat.2021.122735>
- Kanitpong K, Bahia HU (2003) Role of adhesion and thin film tackiness of asphalt binders in moisture damage of HMA. *Asphalt Paving Technol* 72:502–528
- Kavussi A, Naderi B (2020) Application of SCB test and surface free energy method in evaluating crack resistance of SBS modified asphalt mixes. *J Civ Eng Infra* 53(1):103–114. <https://doi.org/10.22059/cej.2019.276295.1555>
- Kavussi A, Qorbani M, Khodaii A, Haghshenas HF (2014) Moisture susceptibility of warm mix asphalt: a statistical analysis of the laboratory testing results. *Constr Build Mater* 52:511–517. <https://doi.org/10.1016/j.conbuildmat.2013.10.073>
- Lee DY, Guinn JA, Khandhal PS, Dunning RL (1990) Absorption of asphalt into porous aggregates. Strategic Highway Research Program (SHRP) Rep. No. SHRP-A/UIR-90–009, National Research Council, Washington, DC
- Ling C, Hanz A, Bahia H (2016) Measuring moisture susceptibility of cold mix asphalt with a modified boiling test based on digital imaging. *Constr Build Mater* 105:391–399. <https://doi.org/10.1016/j.conbuildmat.2015.12.093>
- Liu HY, Jia YQ (2011) Study on the action mechanism of bitumen emulsion and aggregate. *Trans Tech Publ, Adv. Mater. Res*
- Liu W, Yan K, Li QJ, Yang S (2021) Peridynamics-based simulation of semi-circular bending (SCB) testing. *Constr Build Mater* 268:121190. <https://doi.org/10.1016/j.conbuildmat.2020.121190>
- Lue R, Lytton RL (2013) Selective absorption of asphalt binder by limestone aggregates in asphalt mixtures. *J Mater Civ Eng* 25(2):219–226
- Maiha H, Al-Khateeb G (2012) Effect of basalt and limestone aggregate combinations on superpave aggregate properties. The 5th Jordanian International Civil Engineering Conference, Amman, Jordan
- Ribeiro RC, Correia JCG, Seidl PR (2009) The influence of different minerals on the mechanical resistance of asphalt mixtures. *J Petrol Sci Eng* 65(3–4):171–174
- Sadeghi E, Nikudel MR, Khamsehchiyan M, Kavussi A (2022a) A comprehensive view on the compilation of an engineering geological map of carbonate rocks: a case study in the Central Alborz Zone, Iran. *Q J Eng Geol Hydrogeol*. <https://doi.org/10.1144/qjgeh2021-062>
- Sadeghi E, Nikudel MR, Khamsehchiyan M, Kavussi A (2022b) Estimation of unconfined compressive strength (UCS) of carbonate rocks by index mechanical tests and specimen size properties: Central Alborz Zone of Iran. *Rock Mech Rock Eng* 55:125–145
- Taherkhani H (2016) Investigation of asphalt concrete containing glass fibers and nanoclay. *J Civ Eng Infra* 49(1):45–58
- Tan Y, Guo M (2013) Using surface free energy method to study the cohesion and adhesion of asphalt mastic. *Constr Build Mater* 47:254–260
- Wang X, Ren J, Gu X, Li N, Tian Z, Chen H (2021) Investigation of the adhesive and cohesive properties of asphalt, mastic, and mortar in porous asphalt mixtures. *Constr Build Mater* 276:122255
- Watson DE, Moore KA, Williams K, Cooley LA Jr (2003) Refinement of new-generation open-graded friction course mix design. *Transp Res Rec* 1832:78–85
- Yan C, Zhang YU, Bahia H (2020) Comparison between SCB-IFIT, un-notched SCB-IFIT and IDEAL-CT for measuring cracking resistance of asphalt mixtures. *Constr Build Mater* 252:119060. <https://doi.org/10.1016/j.conbuildmat.2020.119060>
- Zaumanis M, Poulidakos LD, Partl MN (2018) Performance-based design of asphalt mixtures and review of key parameters. *Mater Des* 141:185–201. <https://doi.org/10.1016/J.MATDES.2017.12.035>
- Ziari H, Orouei M, Divandari H, Yousefi A (2021) Mechanical characterization of warm mix asphalt mixtures made with RAP and Para-fiber additive. *Constr Build Mater* 279:122456. <https://doi.org/10.1016/j.conbuildmat.2021.122456>